


## RESEARCH ARTICLE

## Sebacic acid as corrosion inhibitor for hot-dip galvanized (HDG) steel in 0.1 M NaCl

Michele Fedel<sup>1</sup>  | Mireille Poelman<sup>2</sup> | Marjorie Olivier<sup>2,3</sup> | Flavio Deflorian<sup>1</sup><sup>1</sup>Department of Industrial Engineering, University of Trento, Trento, Italy<sup>2</sup>Materia Nova, Parc Initialis, Mons, Belgium<sup>3</sup>Materials Science Department, University of Mons (UMONS), Mons, Belgium

## Correspondence

M. Fedel, Department of Industrial Engineering, University of Trento, Via Sommarive n.9, 38123 Trento, Italy. Email: michele.fedel@unitn.it

The potential of sebacic acid as a corrosion inhibitor for hot-dip galvanized steel in 0.1 M NaCl solution has been investigated. Different concentrations of the organic acid have been tested in order to understand the inhibition mechanism of the compound. The electrochemical test revealed a competitive mechanism between the dissolution of the metal in the acidified solution and the inhibition provided by the dicarboxylic species. The formation of a whitish layer consisting of zinc carboxylates and corrosion products was proved by means of scanning electron microscopy (SEM) investigation combined with Fourier transform infrared (FT-IR) analysis. A bidentate bridging coordination between the Zn(II) and the carboxylic species is suggested.

## KEYWORDS

EIS, FT-IR, organic corrosion inhibitors, sebacic acid

## 1 | INTRODUCTION

Galvanizing is the most important application of zinc since nearly half of the production of this metal is used for coatings.<sup>1</sup> Hot-dip galvanizing (HDG) is a particularly effective and efficient application method for zinc coatings because of its relatively low cost and ease of application.<sup>2</sup> In addition, it is considered resource savings and waste avoiding thanks to the recyclability of zinc.<sup>3</sup> HDG is a process promoting the formation of an alloy coating of zinc, which thoroughly covers the steel by immersion in a melt zinc.<sup>4</sup> According to the Zn-Fe phase diagram collected by Massalski et al.,<sup>5</sup> upon solidification, different iron-zinc intermetallic phases are formed throughout the layer.<sup>6</sup> The phase formed on the top of the coating (namely “ $\eta$ ” phase) consists in a solid solution of iron in hexagonal close-packed (HCP) zinc (iron solubility  $\leq 0.03$  wt%).<sup>7</sup> This almost pure Zn layer provides the steel substrate with improved corrosion resistance,<sup>8</sup> thanks to the formation of a protective basic zinc carbonate ( $\text{Zn}_5(\text{CO}_3)_2(\text{OH})_6$ ) on the top of the surface upon interaction with the environment.<sup>9,10</sup> However, in wet or industrial atmospheres as well as in locations near sea level subjected to salt spray, the galvanized layer is prone to corrosion.<sup>9</sup> In these environments, Persson et al.<sup>11</sup> proved that  $\text{Zn}_5(\text{OH})_8\text{Cl}_2\cdot\text{H}_2\text{O}$ ,  $(\text{Zn}(\text{OH})_2)_3\cdot\text{ZnSO}_4\cdot n\text{H}_2\text{O}$ , and  $\text{NaZn}_4(\text{SO}_4)(\text{OH})_6\text{Cl}\cdot 6\text{H}_2\text{O}$  are formed in addition to the basic zinc hydroxycarbonate. To increase the durability of the galvanized layer in such environments, corrosion inhibitors

are often employed. Inorganic compounds are commonly used to promote the formation of a conversion layer of hardly soluble compounds on the galvanized steel surface. Among them, conversion coatings based on molybdates ( $\text{MoO}_4^{2-}$ ),<sup>12,13</sup> tungstates ( $\text{WO}_4^{2-}$ ),<sup>14,15</sup> lanthanides (Ce, La),<sup>16–21</sup> silicates ( $\text{Na}_2\text{SiO}_3$ ,  $\text{K}_2\text{SiO}_3$ ),<sup>22,23</sup> trivalent chromium (Cr (III)),<sup>24</sup> titanium and zirconium (Ti, Zr),<sup>25,26</sup> *n*-tetradecanephosphonic acids,<sup>27</sup> and phosphates ( $\text{PO}_4^{3-}$ )<sup>28,29</sup> have been tested on zinc substrate.

On the other hand, organic corrosion inhibitors can be also employed to suppress galvanized steel corrosion, as they are recognized to (a) be chemically absorbed on metal substrate or (b) to form a thin organic layer of insoluble complexes.<sup>30</sup> In the first case (a), corrosion protection is provided thanks to a decrease in polarization rate because of the presence of several monolayers of organic species that change the structure of the double layer at the metal interface. In the latter case (b), the decrease in corrosion rate is attributed to the capability of the film to block anodic and cathodic active sites and to promote a drop of electroactive species transport rate to or from the metal surface.<sup>31</sup>

Many different organic compounds have been investigated as potential corrosion inhibitors for zinc substrates. They are, for example, polyethylene glycol,<sup>32</sup> pyrrole derived,<sup>33</sup> organic onium compounds,<sup>34</sup> 8-hydroxyquinoline,<sup>35</sup> amines,<sup>36</sup> salicylideneaniline,<sup>37</sup> benzotriazoles,<sup>38</sup> phytic acid,<sup>39</sup> surfactants,<sup>40,41</sup> sulfonates,<sup>42</sup> and

carboxylates.<sup>43-45</sup> Among them, the latter are investigated mainly in the form of salts of weak acids<sup>46-48</sup> thanks to their relatively good solubility in water and inhibition efficiency. On the contrary, little investigation has been carried out on simple weak mono- or dicarboxylic acids as corrosion inhibitors.<sup>49,50</sup> However, new insights into the fundamental interaction mechanism between metallic substrates and carboxylic groups have been already provided by P. Taheri et al.<sup>51,52</sup> studying succinic acid adsorption on metal surface. To our best knowledge, among the different carboxyl-based corrosion inhibitors, sebacic acid (decanedioic acid, C<sub>10</sub>H<sub>18</sub>O<sub>4</sub>, Figure 1) has not been the object of a detailed electrochemical investigation as a potential corrosion inhibitor for HDG steel. Remarkably cheaper compared with the corresponding salt (disodium sebacate, C<sub>10</sub>H<sub>16</sub>Na<sub>2</sub>O<sub>4</sub>), sebacic acid shows a relatively low solubility in water (<1 g/l at room temperature) and pK<sub>1</sub> and pK<sub>2</sub> values of 4.59 and 5.59,<sup>53</sup> respectively. The aim of the present manuscript is to evaluate the potential of sebacic acid as a corrosion inhibitor for HDG steel in 0.1 M NaCl solution. The effect of the inhibitor concentration on the electrochemical response and surface morphology of HDG plates immersed in 0.1 M NaCl solution has been assessed. The evolution of HDG electrodes immersed in the inhibitor-containing solution has been monitored by means of electrochemical impedance spectroscopy (EIS). Fourier

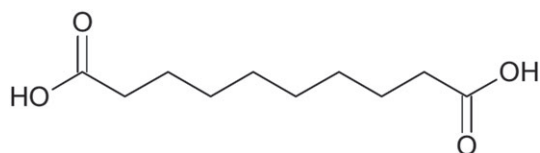


**FIGURE 1** Sebacic acid, HOOC (CH<sub>2</sub>)<sub>8</sub>COOH

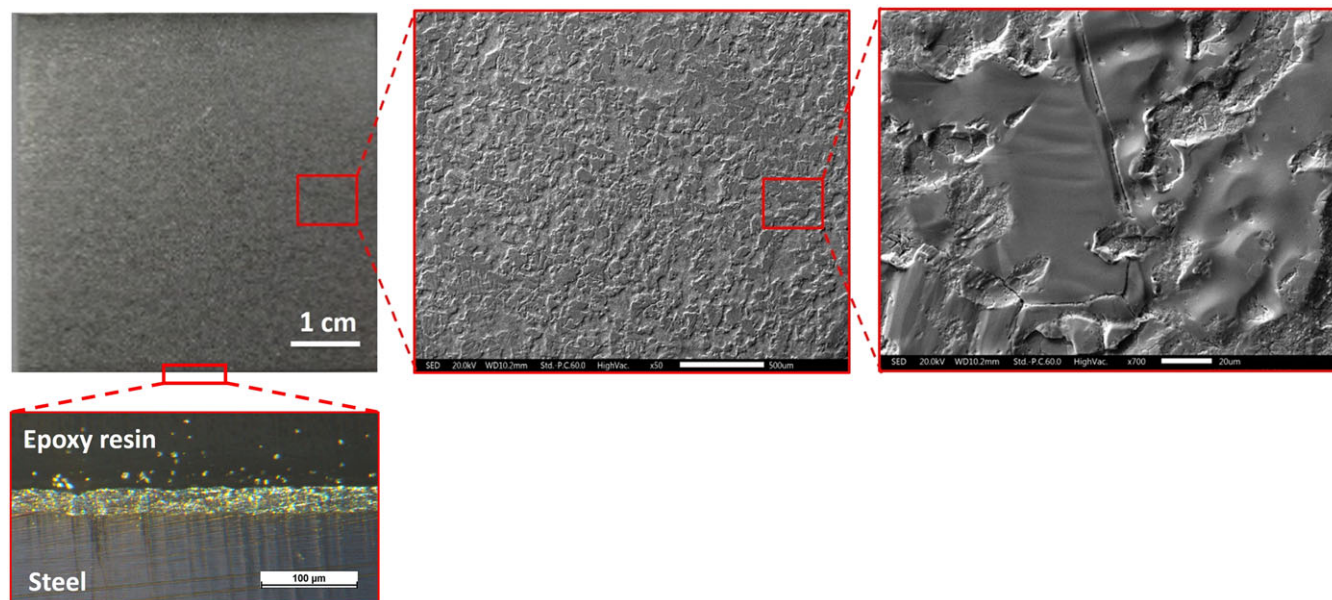


**FIGURE 2** Appearance of the hot-dip galvanized (HDG) substrate

**TABLE 1** Investigated sebacic acid concentrations

	Molar concentration of sebacic acid in 0.1 M NaCl					
	0 M	10 <sup>-4</sup> M	2.5 × 10 <sup>-4</sup> M	5 × 10 <sup>-4</sup> M	7.5 × 10 <sup>-4</sup> M	10 <sup>-3</sup> M
pH	6.4	5.8	4.0	3.9	3.8	3.7

transform Infrared (FT-IR) spectroscopy in attenuated total reflection (ATR) geometry has been employed in order to investigate the formation of carboxylic compounds on the surface of the HDG plates. The morphology and the elemental composition of the HDG steel surface after exposure have been assessed by means of scanning electron microscopy (SEM) and energy dispersive X-rays spectroscopy (EDXS).

## 2 | EXPERIMENTAL

The metallic substrates were cut (50 mm × 50 mm) from continuous HDG steel sheets (0.15 wt.% Al, balance zinc) supplied by ArcelorMittal (Belgium). Sebacic acid was purchased from Merck (Darmstadt, Germany) and used as received without further purification. The substrates were cleaned with acetone under sonication for 10 minutes. Afterwards, the samples were rinsed with deionized water and further dried with pulsed air at ambient temperature. Subsequently, the samples were immersed in a 5 wt% NaOH solution maintained at 60°C for 6 minutes. The samples were then rinsed with deionized water and further dried with blowing nitrogen at ambient temperature. Figure 2 shows the appearance of the substrate after the pre-treatment.

All the electrochemical measurements were collected in 0.1 M NaCl, simply and in combination with different concentrations of sebacic acid (Table 1). For comparison, the electrochemical tests were performed also in 0.1 M NaCl solution modifying the pH adding HCl according to the values indicated in Table 1. The electrochemical tests were carried out using a three electrodes arrangement with a Metrohm AUTOLAB 302 N equipment. A platinum ring and an

Ag/AgCl electrode (3 M KCl, +0.210 V vs standard hydrogen electrode [SHE]) were used as counter and reference electrode, respectively, while the HDG steel coupon was the working electrode. The electrochemical tests were carried out employing an Avesta cell<sup>54</sup> in order to control the temperature, which was maintained at 20°C ± 2°C. The analyzed circular area was about 1 cm<sup>2</sup>. EIS measurements were performed to assess the evolution of the electrode surface exposed to the sebacic acid-containing solution for 24 hours. EIS spectra were collected at the open-circuit potential (OCP), which was measured before each single measurement and potentiostatically maintained during spectrum acquisition. The alternating current (AC) perturbation amplitude was 10 mV (rms), the frequency range between 10<sup>5</sup>–10<sup>2</sup> Hz. Five points per decade were collected. The electrochemical results were obtained from at least two testing samples to ensure reproducibility. ZsimpWin software was employed to fit the experimental spectra. The surface of the samples after exposure to sebacic acid was characterized by means of an ATR infrared spectroscopy equipment (Varian 4100 Excalibur Series) exploiting a diamond internal reflective element (IRE). The wavenumber range was 500 to 4000 cm<sup>-1</sup> and the resolution was 4 cm<sup>-1</sup>. The appearance of the HDG electrodes after immersion in the different solutions was investigated by means of a Jeol JSM-IT300 SEM.

### 3 | RESULTS AND DISCUSSION

Table 1 shows the pH values measured for the solutions employed in the present study. As the sebacic acid concentration increases in the 0.1 M NaCl solution, the pH decreases according to the acid dissociation constant. Notice that all the investigated solutions have a pH

value between 3.7 and 6.4: according to the Eh-pH diagram of Zn,<sup>55</sup> the metal is active (dissolution through formation of Zn<sup>2+</sup> ions), between hydrogen and oxygen reduction limits, in this pH range. Moreover, zinc oxide and zinc oxide hydroxide are both amphoteric compounds, which are recognized to be positively charged when immersed in a water based solution in the investigated pH range.<sup>56,57</sup>

A certain interaction between the negatively charged carboxylic groups and the positively charged surface is therefore expected in these conditions. Figure 3 shows the Nyquist plots during 24 hours of immersion of the HDG electrodes immersed in the 0.1 M NaCl solution at diverse pH levels (Figure 3D is representative of pH values 3.9, 3.8, and 3.7, which show identical response). These plots are reported for comparison, in order to highlight the effect of the acidic pH itself (without adding any different anion to the electrolyte) on the electrochemical response of the HDG substrate. Notice that regardless of the pH level, the HDG electrodes show a quite similar behavior. The electrochemical response of zinc in aqueous media is recognized to be particularly complex because it involves three parallel dissolution paths and the effect of three different adsorbates.<sup>58</sup> In this case, two partially overlapped capacitive loops in the high and middle frequency range ( $\tau_{HF}$  and  $\tau_{MF}$ , respectively) and an inductive loop in the low frequency range ( $\tau_{LF}$ ) are observed. According to previous studies, the previously cited capacitive loops can be attributed to the formation of the contribution of a corrosion product layer composed of zinc compounds (hydroxyl-chlorides and/or oxides) and to faradic process (charge transfer and electrical double layer formation).<sup>23</sup> In addition, during the very first hours of immersion, a pretty much defined inductive loop is observed for all samples in the low frequency range. The appearance of the inductive loop has been attributed to the relaxation of adsorbed intermediate species such as Zn<sup>+</sup><sub>ads</sub>, Zn<sup>2+</sup><sub>ads</sub>, and/or

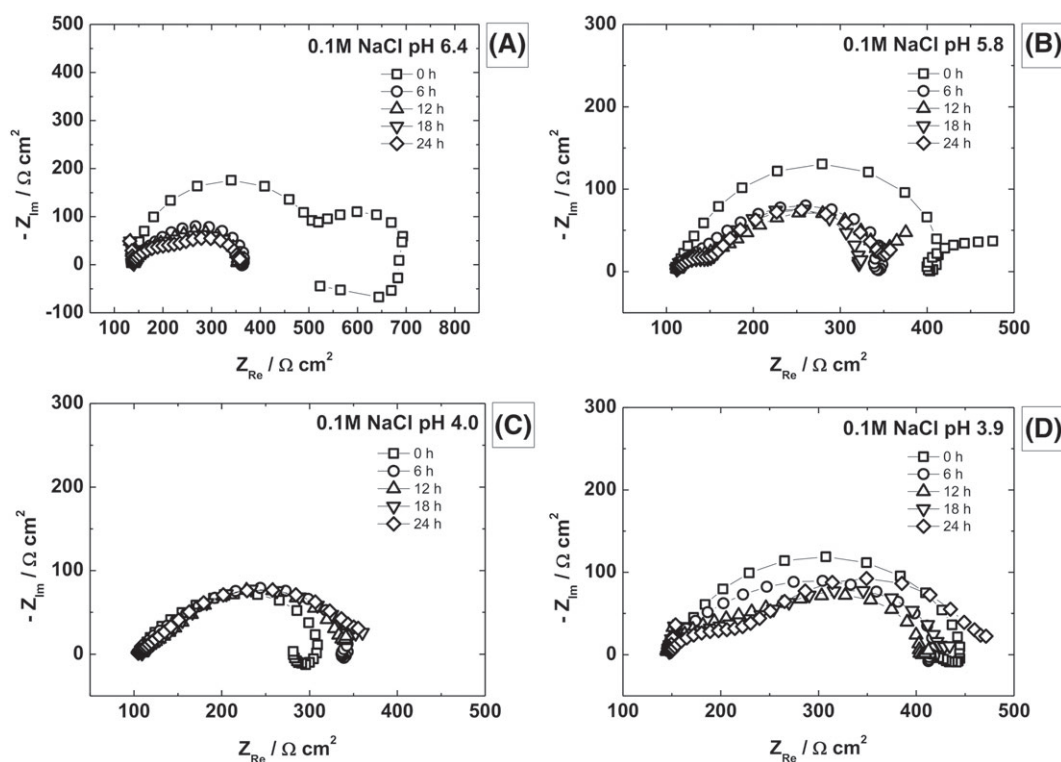


**FIGURE 3** Electrochemical impedance spectroscopy (EIS) plots during immersion in 0.1 M NaCl and different pH: (A) pH = 6.4, (B) pH = 5.8, (C) pH = 4.0, and (D) pH = 3.9 (representative also of pH 3.8 and 3.7)

ZnOH<sub>ads</sub> by C. Cachet and co-workers.<sup>58,59</sup> After the very first hours of immersion, the electrochemical response of the HDG electrodes exposed to different pH levels looks very similar: (a) two relaxation processes can be observed (attributed to the previously describe processes); (b)  $Z_{Re}$  values fall within the 300 to 400  $\Omega\text{cm}^2$  range. Since the behavior of the HDG electrodes immersed in the diverse solution seems to be not remarkably different, the electrolyte consisting in neutral 0.1 M NaCl will be used throughout the paper to compare with the effect of the sebacic acid-containing solutions.

The effect of the presence of the sebacic acid on the corrosion kinetic of HDG has been investigated by means of EIS for 24 hours. The samples have been immersed in the diverse sebacic acid-containing solutions and the evolution of the EIS spectra has been monitored. Figure 4 shows the Nyquist plots for the HDG electrodes immersed in the different solutions. The HDG electrodes immersed in the simply 0.1 M NaCl solution as well as the one immersed in combination with  $10^{-4}$  M sebacic acid behaves similarly. The impedance

values sharply decrease after the very first minutes of immersion, reaching very low values.

The presence of  $10^{-4}$  M sebacic acid seems not to remarkably affect the electrochemical properties of the HDG electrode in the 0.1 M NaCl solution. On the other hand, the impedance spectra of the electrodes immersed in the electrolytes containing  $2.5 \cdot 10^{-4}$  M,  $5 \cdot 10^{-4}$  M, and  $7.5 \cdot 10^{-4}$  M show a remarkably different behavior. The electrodes immersed in such solutions show two clearly distinguishable time constants in the high and middle frequency ranges, respectively. A continuous increase in the magnitude of both the two capacitive loops is observed during all immersion time. The HDG electrode that shows the highest impedance values is the one immersed in  $5 \cdot 10^{-4}$  M sebacic acid solution. The sample immersed in  $10^{-3}$  M sebacic acid solution shows a slight increase in impedance during the first hours of immersion and then remains almost constant. The appearance of the samples after 24 hours of immersion in the diverse solutions is reported in Figure 5. The macroscopic appearance of the

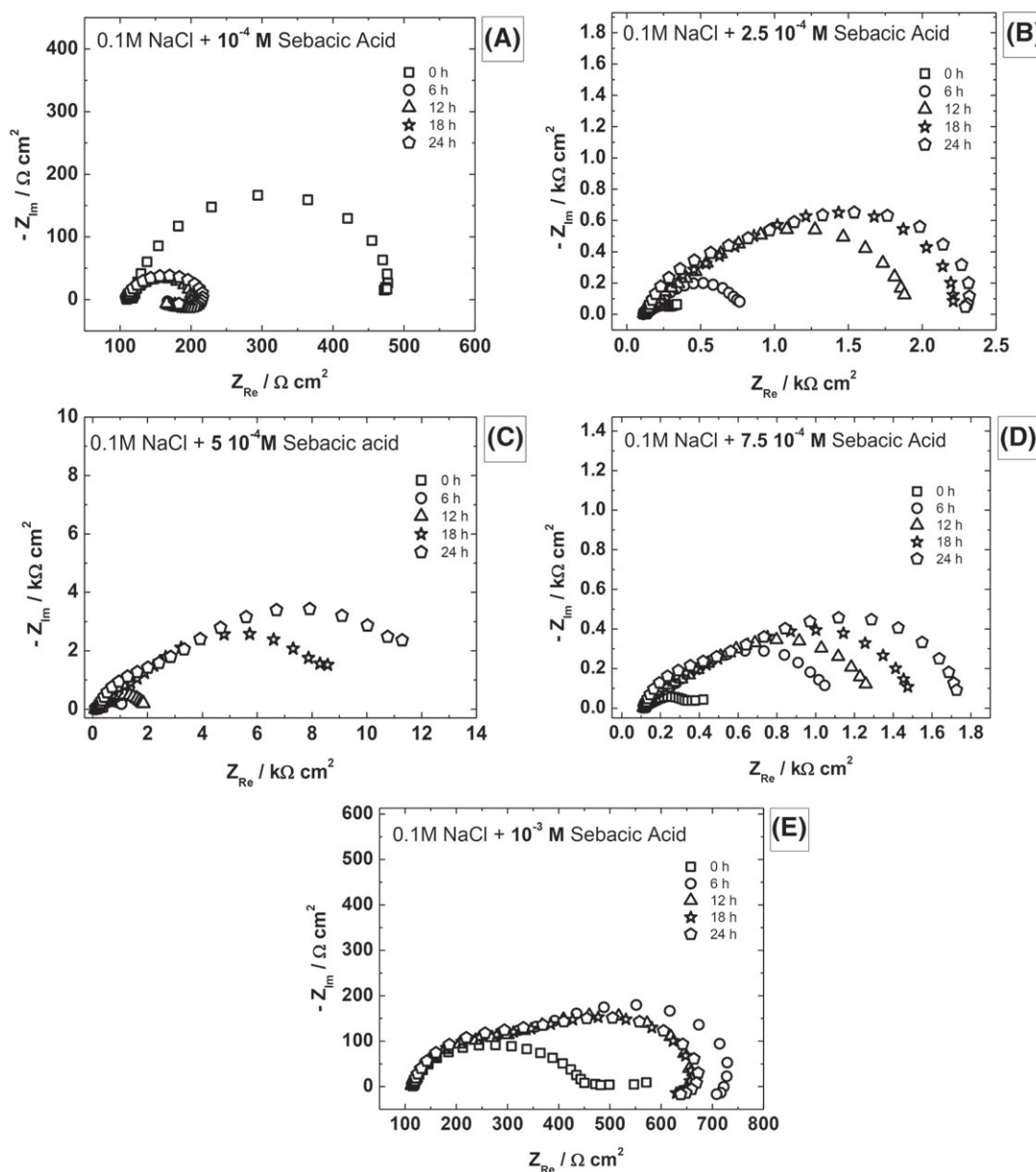


**FIGURE 4** Electrochemical impedance spectroscopy (EIS) plots during immersion in 0.1 M NaCl and different concentrations of sebacic acid: (A)  $10^{-4}$  M, (B)  $2.5 \cdot 10^{-4}$  M, (C)  $5 \cdot 10^{-4}$  M, (D)  $7.5 \cdot 10^{-4}$  M, and (E)  $10^{-3}$  M

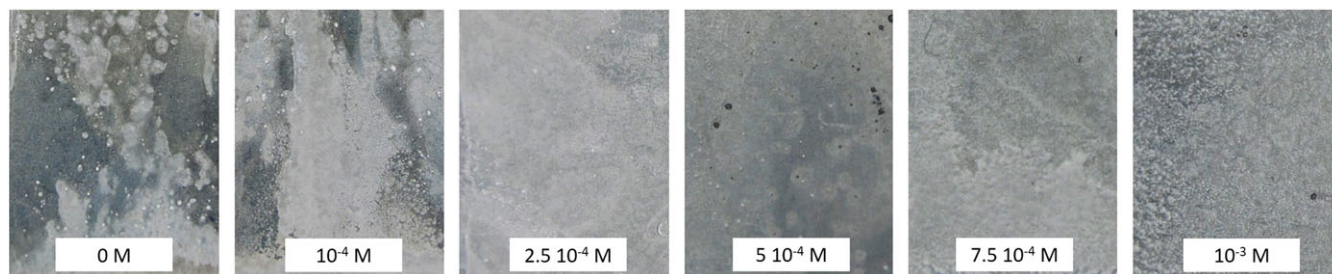


**FIGURE 5** Appearance of the investigated samples after 24 hours of immersion in 0.1 M NaCl solution with various amounts of sebacic acid [Colour figure can be viewed at [wileyonlinelibrary.com](http://wileyonlinelibrary.com)]

corrosion products does not highlight remarkable differences among the HDG panels immersed in the diverse solutions: A whitish layer is always present over the metallic surface. However, one can notice that the HDG coupons exposed in 0.1 M NaCl solution, simply and in combination with  $10^{-4}$  M sebacic acid, show the more relevant extent of corrosion among the studied samples. Low concentration of sebacic acid in the solution seems therefore not beneficial to provide the Zn substrate with improved corrosion resistance. Many distributed corrosion attacks can be observed on these electrodes after exposure. On the other hand, the HDG plates immersed in the electrolyte containing  $2.5 \cdot 10^{-4}$  M  $\div$   $10^{-3}$  M sebacic acid show an almost homogeneous layer of white compounds on the electrode surface without signs of strong corrosion attacks. To get more insight into the composition and morphological features of the whitish layer formed in presence of sebacic acid, SEM observations and EDXS analyses have been performed. Figure 6 depicts the appearance of the surface of the sample exposed in the solution containing  $5 \cdot 10^{-4}$  M sebacic acid for 24 hours observed by SEM. Secondary electrons (Figure 6A) and back-scattered electrons (Figure 6B) images highlight the presence of a tridimensional needles shaped layer on the zinc surface. The EDXS analysis indicates that high amounts of carbon are present on the surface, thus suggesting that the whitish layer observed in Figure 5 consists in a mixture of zinc carboxylates and zinc corrosion products. These features will be further investigated by means of infrared spectroscopy.

According to EIS results and the evidences from SEM observations, a deeper analysis of the impedance spectra has been carried out for the HDG sample exposed to the solution containing  $5 \cdot 10^{-4}$  M sebacic acid, which showed the highest increase in impedance during the 24 hours of immersion. For comparison, also the HDG plate immersed in simply 0.1 M NaCl solution (pH = 6.4) has been the object of a deeper analysis. For this purpose, the EIS spectra have been fitted by means of electrical equivalent circuits (e.c.c.). The correct attribution of the two capacitive loop observed for the sample immersed in neutral 0.1 M NaCl solution is controversial. Some authors<sup>35,39,42</sup> assign the high-frequency time constant to the faradic process described by a charge transfer resistance and a double layer capacitance (sometimes substituted by a constant phase element [CPE]), while the middle-frequency time constant to the contribution of the corrosion product layer. However, other authors<sup>23,40,60,61</sup> suggest the opposite.

In this work, the electrochemical behavior of HDG plates exposed to 0.1 M NaCl solution has been modeled employing the e.c.c. depicted in Figure 7A (according to previous studies<sup>35,39,42</sup>):  $R_{sol}$  stands for the electrolyte resistance while the layer of corrosion

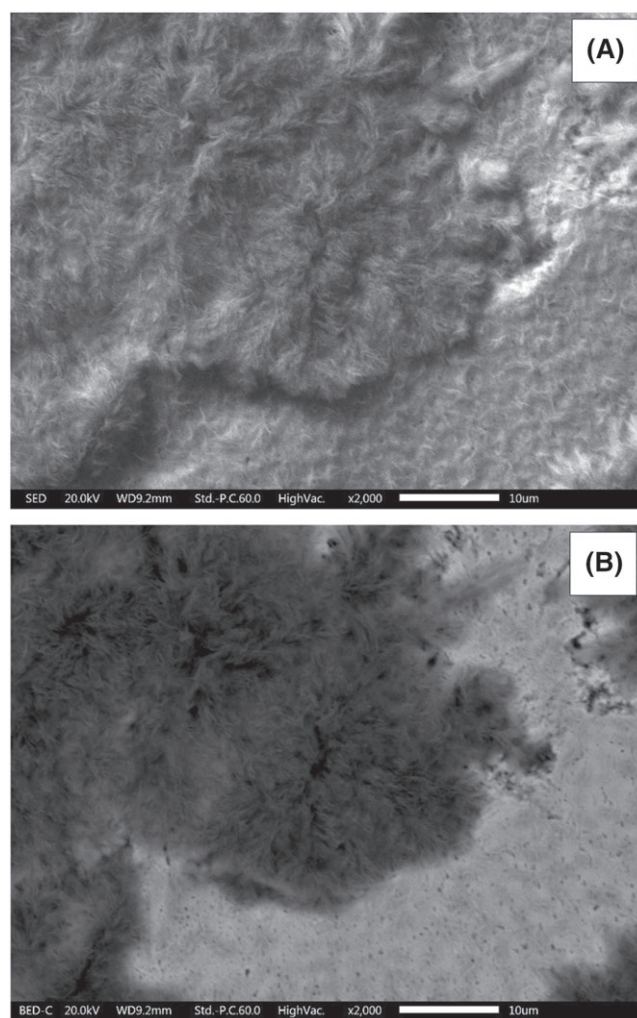


**FIGURE 6** Appearance of the sample immersed in 0.1 M NaCl +  $5 \cdot 10^{-4}$  M sebacic acid during 24 h: (A) Secondary Electrons (SE) and (B) Backscattered electrons (BSE)

products deposited on the electrode surface has been modeled using a resistance ( $R_{Deposit}$ ) and a CPE ( $CPE_{Deposit}$ ).  $R_{ct}$  has been introduced to account for the charge transfer resistance while the  $CPE_{dl}$  has been attributed to the dielectric contribution of the electrochemical double layer. The inductive behavior observed during the very first minutes of immersion (which have been attributed to the adsorbed intermediate species such as  $Zn^+_{ads}$  and/or  $ZnOH_{ads}$ <sup>58,59</sup>) has not been considered and the very first spectra (corresponding to “time = 0”) have not been modeled. As far as the HDG plates exposed to 0.1 M NaCl +  $5 \cdot 10^{-4}$  M sebacic acid solution are concerned, the e.c.c. depicted in Figure 7B

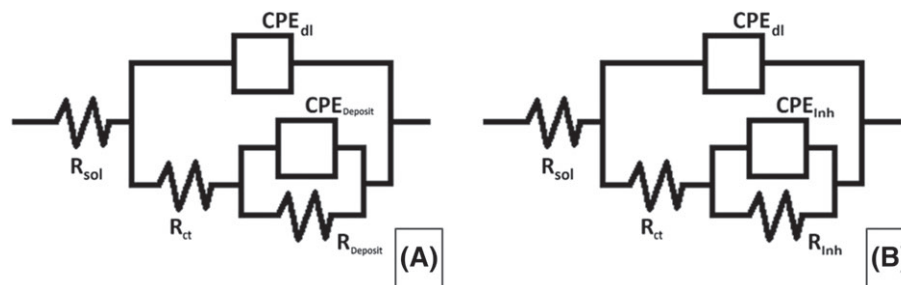


**FIGURE 7** Electrical equivalent circuit employed to fit the experimental curves of the hot-dip galvanized (HDG) panels immersed (A) in simply 0.1 M NaCl solution and (B) in combination with  $5 \cdot 10^{-4}$  M sebacic acid

has been employed.  $R_{sol}$  stands for the electrolyte resistance, the layer of inhibitor and corrosion products has been modeled using a resistance ( $R_{inh}$ ) and a CPE ( $CPE_{inh}$ ). Similarly, the faradic process at the interface has been described using a resistance and a CPE ( $R_{ct}$  and  $CPE_{dl}$ , respectively). In both circuits in Figure 7, CPEs have been used instead of pure capacitance, according to the relationship<sup>62</sup>:  $Z_{CPE} = [Q \cdot (\omega)^{\alpha}]^{-1}$ , where the parameters “Q” and “ $\alpha$ ” are the pre-exponential factor and the exponent of the CPE, respectively. Figure 8 shows the evolution with immersion time of the electrical equivalent parameters attributed to the corrosion products ( $R_{Deposit}$ ,  $CPE_{Deposit}$ ) and to the mixture carboxylic compounds and corrosion products ( $R_{inh}$ ,  $CPE_{inh}$ ). Notice that  $R_{inh}$  increases during immersion

time from  $10^3 \Omega \text{cm}^2$  to about  $10^4 \Omega \text{cm}^2$ , according to the formation of a protective layer on the HDG sample. The resistance attributed to the corrosion products of HDG surface immersed in simple 0.1 M NaCl,  $R_{Deposit}$ , shows remarkably lower values, about  $10^2 \Omega \text{cm}^2$ , thus suggesting the poor protective effect of the layer.

The pre-exponential factor  $Q_{inh}$  decreases during immersion time from about  $10^{-3} \text{ s}^{\alpha} \Omega^{-1} \text{ cm}^{-2}$  to  $10^{-4} \text{ s}^{\alpha} \Omega^{-1} \text{ cm}^{-2}$  during 24 hours. The value of the exponent  $\alpha$  related to the  $CPE_{inh}$  ranges from 0.5 to 0.7 during immersion time. Therefore, the physical meaning of the pre-factor cannot be univocally determined, even if it is likely to be strongly connected to the dielectric properties of the protective layer.

Figure 9 shows the comparison of the  $R_{ct}$  and  $Q_{dl}$  values obtained from the fitting of the experimental spectra for the samples immersed in the electrolytes under investigation. From Figure 9A, it is possible to observe that the charge transfer resistance of the samples immersed in the solution containing sebacic acid increases from about 30 to  $4 \cdot 10^3 \Omega \text{cm}^2$  during immersion time.  $R_{ct}$  trend is the same of the resistance attributed to the protective layer formed thanks to the presence of the carboxylic species in the solution. On the other hand, the charge transfer resistance for the HDG plate immersed in simply 0.1 M NaCl solution remains almost stable at about  $10^2 \Omega \text{cm}^2$  in accordance with the noticeable corrosion attacks observed on the sample (see Figure 5). As far as the pre-factor and the exponent related to the CPEs employed to model the interface are concerned, notice that  $\alpha$  is included in the range  $0.9 \div 0.8$  for the electrode exposed to the solution containing the carboxylic acid, while it scatters from 0.7 to 0.8 for the electrode immersed in the simply 0.1 M NaCl solution. The high values of the pre-exponential factors of the  $CPE_{dl}$  ( $10^{-4} \div 10^{-5} \text{ s}^{\alpha} \Omega^{-1} \text{ cm}^{-2}$ ) as well as the scattered  $\alpha$  values ( $0.9 \div 0.8$ ) suggest that the  $CPE_{dl}$  cannot be assumed to correspond to an ideal double layer capacitance. According to the literature,<sup>58–60</sup> the regressed parameters of CPEs used to fit impedance measurements exhibiting frequency dispersion do not necessarily have a clear physical meaning, even if a good fit can be obtained. In fact, the CPE is associated with a distribution of time constants on the electrode surface and has been attributed to the presence of surface heterogeneity, roughness, or to a distribution of time constants for charge-transfer reactions.<sup>61,62</sup> In fact, when the exponent of the CPE is between 0.5 and 1, its real physical meaning is controversial and object of debate.<sup>63–67</sup> It is likely that the  $CPE_{dl}$  is strongly affected by the roughness and the surface heterogeneity of the metal electrode. In addition, it is not excluded that the model is not able to efficiently separate the contribution of the double layer from the corrosion products.

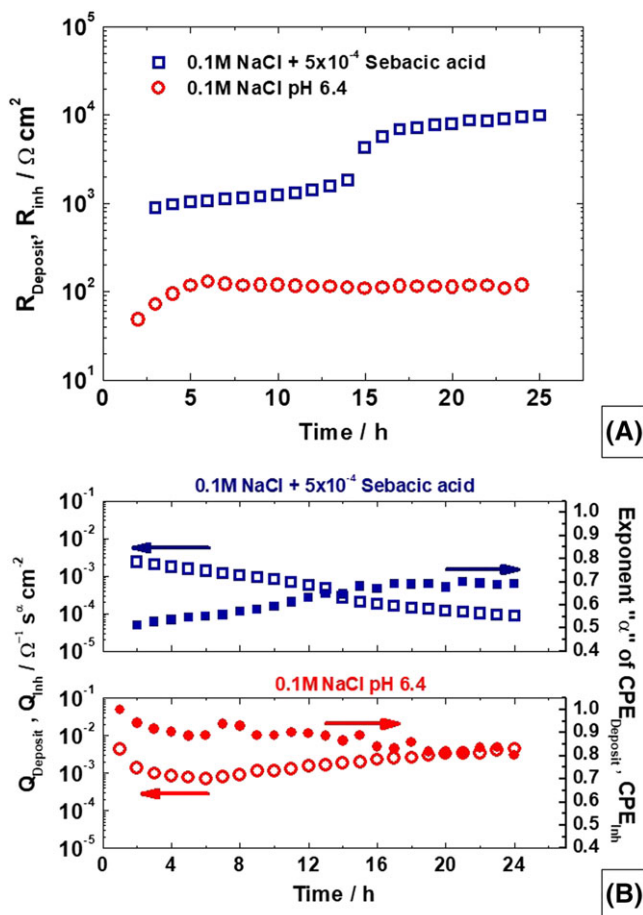


**FIGURE 8** Evolution of  $R_{inh}$  (A) and the “pre-factor” (empty symbol) and “exponent” (full symbol) related to  $CPE_{inh}$  (B) for the sample immersed in 0.1 M NaCl +  $5 \cdot 10^{-4}$  M sebacic acid during 24 h

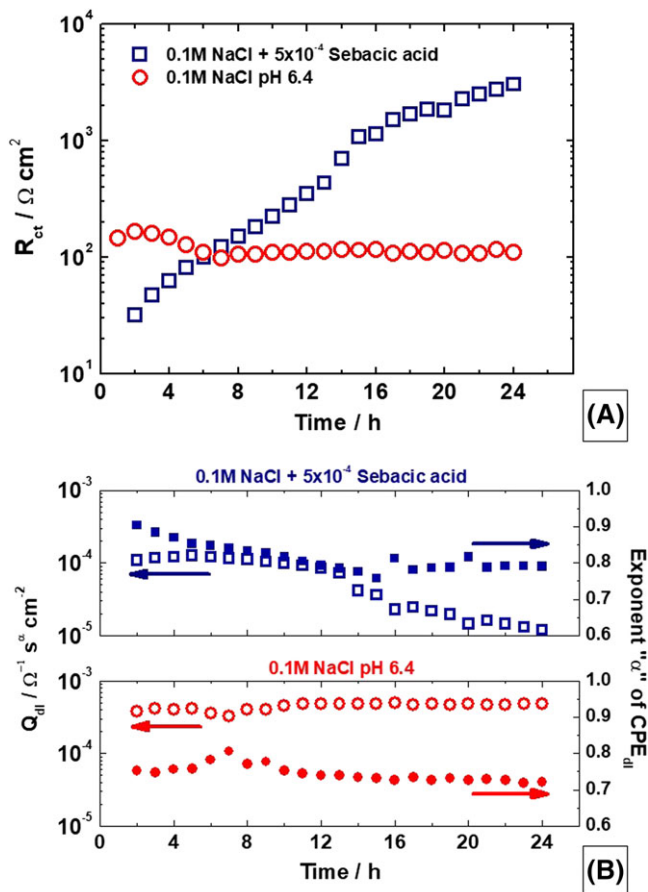
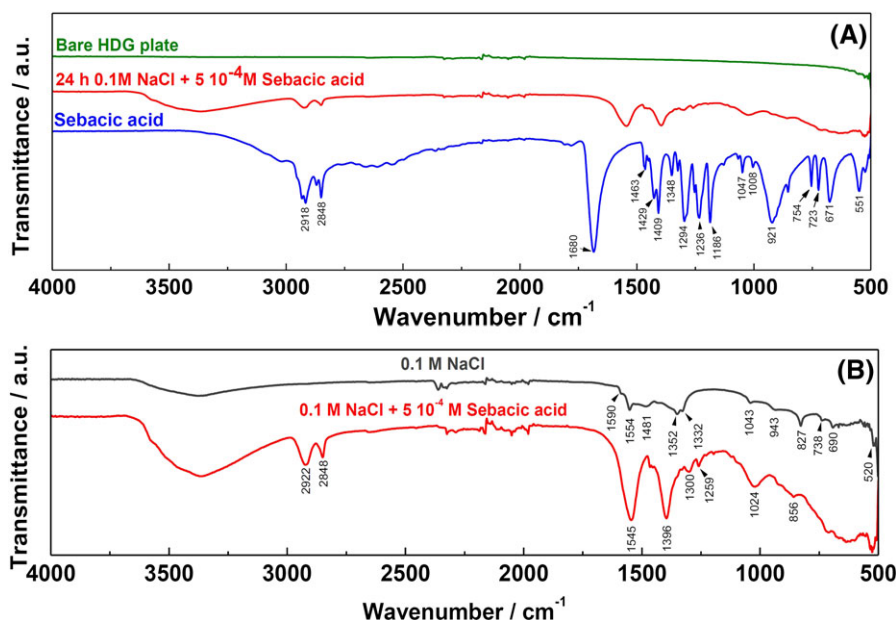


**FIGURE 9** Evolution of  $R_{ct}$  (A) and the “pre-factor” (empty symbol) and “exponent” (full symbol) related to  $CPE_{int}$  (B) for the sample immersed in 0.1 M NaCl +  $5 \cdot 10^{-4}$  M sebacic acid during 24 hours

Infrared spectroscopy has been employed to investigate the composition of the layer formed on the HDG plates upon immersion in the different solutions. Figure 10 shows the comparison between the ATR FT-IR spectra of the pure sebacic acid and the surface of

the HDG plate immersed for 24 hours in the solution containing 0.1 M NaCl +  $5 \cdot 10^{-4}$  M sebacic acid. For comparison, also the spectrum collected over the bare HDG sample is reported. In the sebacic acid spectrum, the characteristic peaks of carboxylic acid are present. In particular, notice the sharp absorption band at  $1680 \text{ cm}^{-1}$  corresponding to C = O asymmetric stretch. The peaks observed in the domain of  $2848 \text{ cm}^{-1}$  and  $2918 \text{ cm}^{-1}$  are attributed to asymmetric and symmetric stretching of the methylene group  $\text{CH}_2$ , respectively. Similarly, the peaks at  $1421 \text{ cm}^{-1}$  and  $723 \text{ cm}^{-1}$  are attributed to the bending and the swinging vibration of the  $\text{CH}_2$  as well as the peaks at  $1297 \text{ cm}^{-1}$ ,  $1233 \text{ cm}^{-1}$ , and  $1186 \text{ cm}^{-1}$  assigned to  $\text{CH}_2$  wagging. The strong peak at  $921 \text{ cm}^{-1}$  is attributed to OH vibrations.

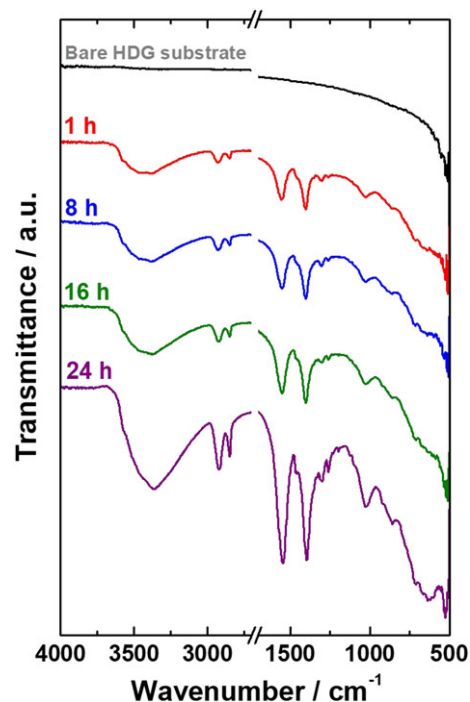
The comparison between the infrared spectrum for the HDG sample immersed in simply 0.1 M NaCl and in combination with sebacic acid is reported in Figure 10B. The infrared spectrum of the HDG plates exposed to simply 0.1 M NaCl shows the presence of hydrozincite ( $\text{Zn}_5(\text{CO}_3)_2(\text{OH})_6$ ) as suggested by the peaks at  $827 \text{ cm}^{-1}$ ,  $943 \text{ cm}^{-1}$ ,  $1043 \text{ cm}^{-1}$ ; the carbonate peaks at  $1352 \text{ cm}^{-1}$ ,  $1481 \text{ cm}^{-1}$ ,  $1554 \text{ cm}^{-1}$ ; and the shoulder at  $1332 \text{ cm}^{-1}$ .<sup>68-71</sup> The OH contribution is clearly observed in the range  $3200$  to  $3600 \text{ cm}^{-1}$ .<sup>72</sup> It is not possible to exclude the presence of small amounts of simonkolleite ( $\text{Zn}_5(\text{OH})_8\text{Cl}_2 \cdot \text{H}_2\text{O}$ ) considering the presence of weak peaks at  $520 \text{ cm}^{-1}$  and  $690 \text{ cm}^{-1}$  as well as the shoulder at  $1590 \text{ cm}^{-1}$ .<sup>73</sup> According to the literature,<sup>74</sup> ZnO is likely to be present on the HDG surface but it cannot be clearly observed by ATR FT-IR because of the absorption in the less than  $650 \text{ cm}^{-1}$  wavenumber range, which makes it identifiable only if it is the most important compound. From Figure 10B, it is possible to identify the presence of the carboxylic acid in the white layer observed on the HDG surface after 24 hours of immersion in 0.1 M NaCl +  $5 \cdot 10^{-4}$  M sebacic acid. Indeed, the corresponding ATR spectrum shows the presence of the peaks attributed to asymmetric and symmetric stretching of the methylene group  $\text{CH}_2$  ( $2848$  and  $2918 \text{ cm}^{-1}$ ) and vibration of  $\text{CH}_2$



**FIGURE 10** Attenuated total reflection (ATR) Fourier transform Infrared (FT-IR) spectra collected over: Bare hot-dip galvanized (HDG) plate, the sample immersed in 0.1 M NaCl +  $5 \cdot 10^{-4}$  M sebacic acid during 24 hours and as received solid sebacic acid

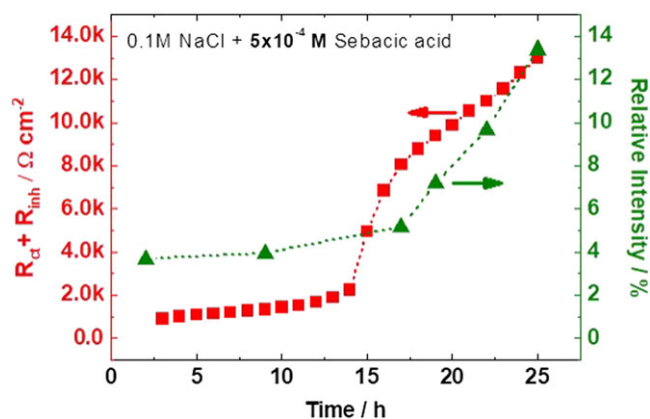
at  $1024\text{ cm}^{-1}$ . The broad band in the  $3200\text{ to }3600\text{ cm}^{-1}$  wavenumber range has been attributed to the OH-group vibration on HDG surface, thus suggesting the presence of hydrozincite and/or residual absorbed water in the whitish layer. The disappearance of the strong absorption at  $1680\text{ cm}^{-1}$  corresponding to C = O asymmetric stretching suggests that undissociated monomers are not present in the whitish layer. In addition, the two strong absorption peaks located at  $1554\text{ cm}^{-1}$  and  $1396\text{ cm}^{-1}$  correspond to asymmetric and symmetric  $\text{COO}^-$  stretching, respectively.<sup>75,76</sup> According to the literature, the previously cited peaks fall within the range of the asymmetric stretching modes of  $\text{CO}_3^{2-}$  devoted to zinc carbonate ( $\text{ZnCO}_3$ ), which are commonly observed at  $1500 \div 1552\text{ cm}^{-1}$  and  $1380 \div 1385\text{ cm}^{-1}$ , respectively.<sup>77-79</sup> Even though a formation of a certain amount of formation of  $\text{ZnCO}_3$  is likely to occur also when the sebacic acid is added to the  $0.1\text{ M NaCl}$  electrolyte, it is believed that the most plausible attribution of the peaks located at  $1554\text{ cm}^{-1}$  and  $1396\text{ cm}^{-1}$  is to  $\text{COO}^-$  stretching. In fact, it has to be considered that (a) the formation of  $\text{ZnCO}_3$  is not compatible with the absence of the out-of-plane deformation mode of  $\text{CO}_3^{2-}$  of  $\text{ZnCO}_3$  located at  $829\text{ cm}^{-1}$ <sup>79</sup>; (b) the medium/strong absorption peaks related to  $\text{CH}_2$  suggest the presence of carboxylic species on the HDG surface. For these reasons, the occurrence of the  $\text{COO}^-$  corresponding peaks seems to confirm the presence of zinc carboxylic compounds on the surface of the HDG steel electrodes. According to the literature,<sup>80,81</sup> the frequency shift ( $\Delta\nu$ ) between  $\nu_{\text{as}}(\text{COO}^-)$  and  $\nu_{\text{s}}(\text{COO}^-)$  can be employed as a spectroscopic criterion to unravel the coordination type of the carboxylate binding. The interactions between  $\text{Zn}^{2+}$  ions and aliphatic acids, leading to the formation of metal carboxylates, potentially form a monodentate ligand, an ionic structure, a bidentate chelate, or a bridging bidentate.<sup>46,68,69,73</sup> In this case, the calculated  $\Delta\nu(\text{COO}^-)$  is equal to  $149\text{ cm}^{-1}$  ( $= 1545\text{ cm}^{-1} - 1396\text{ cm}^{-1}$ ). According to the literature,<sup>82</sup> the bidentate bridging occurs when  $\Delta\nu(\text{COO}^-)_{\text{studied complex}} \leq \Delta\nu(\text{COO}^-)_{\text{sodium salt}}$ . The  $\Delta\nu(\text{COO}^-)$  for the corresponding disodium sebacate (not reported spectrum) has been found to be  $144\text{ cm}^{-1}$ . Considering that in this case,  $\Delta\nu(\text{COO}^-)_{\text{studied complex}}$  almost equal to  $\Delta\nu(\text{COO}^-)_{\text{sodium salt}}$ , we can assume that bidentate bridging coordination takes place between the deprotonated sebacic acid molecules and the  $\text{Zn(II)}$  in the investigated layer. Commonly, the bidentate bridging coordination implies a shift to higher wavenumbers of  $\nu_{\text{as}}(\text{COO}^-)$  and  $\nu_{\text{s}}(\text{COO}^-)$  of the studied complex. In our investigation, this shift has not been observed. For this reason, even if the hypothesis of a bidentate bridging is in accordance with similar study in the literature<sup>51,81</sup> related to Zn/carboxylates interaction, the exact coordination type has not been unequivocally proven by the experimental results.

Figure 11 shows the time evolution of the infrared spectra collected over the HDG plate immersed in the solution containing  $0.1\text{ M NaCl} + 5 \cdot 10^{-4}\text{ M}$  sebacic acid. Notice the increase in intensity of the characteristic peaks with immersion time, in particular, those located at  $1554\text{ cm}^{-1}$  and  $1396\text{ cm}^{-1}$ , which corresponds to  $\text{COO}^-$  stretching. This finding suggests that the formation of a carboxyl/ $\text{Zn}^{2+}$  layer initiates immediately after the immersion of the HDG plate in the solution and continues with time. It is likely that with immersion time, an increasing number of Zn carboxylates layers is formed on the surface of the HDG plate. EIS investigation revealed



**FIGURE 11** Attenuated total reflection (ATR) Fourier transform Infrared (FT-IR) spectra collected over the sample immersed in  $0.1\text{ M NaCl} + 5 \cdot 10^{-4}\text{ M}$  sebacic acid during 24 hours

that also  $R_{\text{ct}}$  and  $R_{\text{inh}}$  increase during immersion time in the solution containing  $0.1\text{ M NaCl} + 5 \cdot 10^{-4}\text{ M}$  sebacic acid. In this sense, the corrosion protection properties of the HDG electrodes seem to be strictly related to the evolution of the carboxylates layer on metal surface. In Figure 11, the evolution of the relative intensity of the ex-situ collected ATR FT-IR peak corresponding to  $\nu_{\text{as}}(\text{COO}^-)$  is overlapped to the sum of  $R_{\text{ct}} + R_{\text{inh}}$  (obtained from EIS). The latter parameter can be considered as an indication of the overall protection offered by the inhibitor, as it includes the resistive contributions of the corrosion product, the carboxylic species, and the interface. The trends reported in Figure 12 are somehow similar. First of all, during the initial  $10 \div 12$  hours, both the relative intensity of the  $\nu_{\text{as}}(\text{COO}^-)$  peak and the sum  $R_{\text{ct}} + R_{\text{inh}}$  only slightly increase. In addition, after



**FIGURE 12** Comparison between the evolution of the relative intensity of the Attenuated total reflection (ATR) Fourier transform Infrared (FT-IR) peak corresponding to  $\nu_{\text{as}}(\text{COO}^-)$  and the sum of  $R_{\text{ct}} + R_{\text{inh}}$



**TABLE 2** Comparison of the inhibition efficiency (IE%) of different organic corrosion inhibitor for HDG steel and zinc in neutral saline media

Inhibitor	Electrolyte	Time	Concentration	IE%	Ref
8-quinolinol	0.5 M NaCl	3 h	$10^{-3}$ M	90-98	48
<i>Mansoa alliacea</i>	3 wt% NaCl	3 h	300 mg/L	92	83
5-amino-1,3,4-thiadiazole-2-thiol	50 mM NaCl	3 h	0.0037mM	60.5	35
2-mercaptobenzothiazole	50mM NaCl	3 h	1.136mM	90.1	35
2,3-dimercapto-1-propanol	0.5 M NaCl	2 h	1mM	97.0	39
Phytic acid + $Mn^{2+}$ + dithio-oxamide	0.5 M NaCl	2 h	0.5:1:1mM	97.9	39
Sodium gluconate	3.0 wt% NaCl	--	$10^{-3}$ M	78.0	40
Cetyltrimethylammonium bromide	3.0 wt% NaCl	--	$2.74 \cdot 10^{-5}$ M	74.0	40
Sodium gluconate + Cetyltrimethylammonium bromide	3.0 wt% NaCl	--	$10^{-3}$ : $2.74 \cdot 10^{-5}$ M	94.0	40
Decanoic acid	ASTM D1387 solution <sup>a</sup>	24 h	0.77 wt%	83.5	43
Decanoic acid	ASTM D1387 solution <sup>a</sup>	24 h	0.77 wt%	93.6 <sup>b</sup>	43
{(2-hydroxyethyl)[(4-methyl-1H-1,2,3-benzotriazol-1-yl)methyl] Amino}ethanol + decanoic acid	ASTM D1387 solution <sup>a</sup>	24 h	0.1 wt%: 0.77 wt%	99.0	50
Sebacic acid	0.1 M NaCl	24 h	$5 \cdot 10^{-4}$ M	98.9	This work

<sup>a</sup>148 mg/l  $Na_2SO_4$ , 165 mg/l NaCl, 138 mg/l  $NaHCO_3$ .

<sup>b</sup>Electroplated steel.

12 ÷ 17 hours, a relevant intensification of the  $v_{as}$  ( $COO^-$ ) peak is accompanied by a rise in the sum  $R_{ct} + R_{inh}$ . Based on these observations, it seems that sebacic acid promotes the formation of a protective layer on HDG surface. The whitish film consists in a mixture of zinc carboxylates and zinc corrosion products (probably hydrozincite), which provide the substrate with improved corrosion protection during immersion in 0.1 M NaCl.

According to the formula reported in previous studies,<sup>39,40,43,83</sup> the corrosion inhibition efficiency of sebacic acid ( $5 \cdot 10^{-4}$  M) in 0.1 M NaCl after 24 hours of immersion has been calculated and has been found to be about 98.9%. The comparison of this finding with literature data related to the efficiency of organic corrosion inhibitor on HDG steel and zinc is reported in Table 2. The calculated inhibition efficiency for  $5 \cdot 10^{-4}$  M sebacic acid is one of the highest among the data reported in the literature. However, one should consider that: (a) the efficiency strongly depends upon the concentration of the sebacic acid; (b) the addition of sebacic acid implies an acidification of the electrolyte, which, in principle, could promote an increase in the corrosion rate; (c) the electrolyte employed in this study (0.1 M NaCl) is more diluted than the average of the electrolytes used in the literature (for this reason, higher inhibition efficiency values are expected). In summary, compared with other organic compounds, sebacic acid has a competitive corrosion inhibition efficiency but a very precise control of the concentration is needed to get a beneficial effect in terms of protection of the HDG substrate. It has to be mentioned that, in any case, even the highest sebacic acid concentration investigated in this study ( $10^{-3}$  M, quite close to the solubility limit) has been demonstrated not to increase the corrosion rate compared with the neutral 0.1 M NaCl blank solution.

## 4 | CONCLUSIONS

The effectiveness of the sebacic acid as corrosion inhibitor for HDG steel in 0.1 M NaCl has been assessed in the present paper. According to the dissociation constant, the presence of carboxylic acid in 0.1 M

NaCl solution promotes a decrease in pH. Considering the concentration of sebacic acid in the range  $10^{-4}$  ÷  $10^{-3}$  M, an intermediate value of about  $5 \cdot 10^{-4}$  M seems to provide HDG substrate with improved corrosion protection. This concentration in carboxylic acid seems to balance the increased corrosion rate caused by the acidification of the saline solution and the healing effect due to the presence of the organic molecule. SEM investigation revealed that for the most efficient sebacic acid concentration, a whitish layer consisting of zinc carboxylates and corrosion products is formed on the HDG plate surface. Ex-situ FT-IR analysis seems to suggest that a bidentate bridging coordination takes place between the Zn(II) and the carboxylic species. However, the shift observed for the symmetric and asymmetric  $COO^-$  stretching are not unequivocally supporting this hypothesis.

Having said this, even if the sebacic acid is hardly soluble in water and promotes a decrease in pH, its relative low cost and corrosion mitigation effectiveness (inhibition efficiency after 24 hours of immersion  $\approx 99\%$ ) makes it a corrosion inhibitor worthy of consideration.

## ORCID

Michele Fedel  <https://orcid.org/0000-0001-6994-0816>

## REFERENCES

- Zhang XJ. *Corrosion and electrochemistry of zinc*. New York: Springer Science+Business Media New York; 1996.
- Burstein GT, Shreir LL, Jarman RA. *Corrosion - Volume 2.: Corrosion Control (3rd Edition)*. Oxford: Butterworth-Heinemann; 2000.
- Maaß P, Peißker P. *Handbook of Hot-Dip Galvanization*. Wiley-VCH Verlag GmbH & Co. KGaA: Weinheim; 2011.
- Kuklík V, Kudláček J. *Hot-Dip Galvanizing of Steel Structures*. Oxford: Butterworth-Heinemann; 2016.
- Massalski TB, Okamoto H, Subramanian PR, Kacprzak L. *Binary alloy phase diagrams 2<sup>nd</sup> ed.* ASM International: Cleveland; 1990.
- Peng S, Xie SK, Yang YM. Aluminum and antimony segregation on a batch hot-dip galvanized Zn-0.05Al-0.2Sb coating. *J Alloys Compd*. 2017;694:1004-1010.
- Marder AR. The metallurgy of zinc-coated steel. *Prog Mater Sci*. 2000;45(3):191-271.

8. Peng S, Xie SK, Lu JT, Zhang LC. Surface characteristics and corrosion resistance of spangle on hot-dip galvanized coating. *J Alloys Compd.* 2017;728:1002-1008.
9. Revie RW (Ed). *Uhlig's Corrosion Handbook*. 2nd ed. Hoboken: John Wiley & Sons; 2000:887.
10. Pistofidis N, Vourlias G, Chaliampalias D, Chrysafis K, Stergioudis G, Polychroniadis EK. On the mechanism of formation of zinc pack coatings. *J Alloys Compd.* 2006;407(1-2):221-225.
11. Persson D, Thierry D, Karlsson O. Corrosion and corrosion products of hot dipped galvanized steel during long term atmospheric exposure at different sites world-wide. *Corros Sci.* 2017;126:152-165.
12. Zhang SH, Yang B, Kong G, Lu JT. Electrochemical analysis of molybdate conversion coating on hot-dip galvanized steel in various growth stages. *Surf Interface Anal.* 2017;49(8):698-704.
13. Liu D, Yang Z, Wang Z, Zhang C. Synthesis and evaluation of corrosion resistance of molybdate-based conversion coatings on electroplated zinc. *Surf Coat Technol.* 2010;205(7):2328-2334.
14. da Silva CG, Correia AN, de Lima-Neto P, Margarit ICP, Mattos OR. Study of conversion coatings obtained from tungstate-phosphoric acid solutions. *Corros Sci.* 2005;47(3):709-722.
15. da Silva CG, Margarit-Mattos ICP, Mattos OR, Perrot H, Tribollet B, Vivier V. The molybdate-zinc conversion process. *Corros Sci.* 2009;51(1):151-158.
16. Hinton BRW. Corrosion inhibition with rare earth metal salts. *J Alloys Compd.* 1992;180(1-2):15-25.
17. Montemor MF, Ferreira MGS. Corrosion performance of a two-step pre-treatment for galvanized steel based on lanthanum nitrate and silanes. *Surf Interface Anal.* 2004;36(8):773-776.
18. Montemor MF, Simões AM, Ferreira MGS. Composition and behaviour of cerium films on galvanised steel. *Prog Org Coat.* 2001;43(4):274-281.
19. Zhang SH, Kong G, Lu JT, Che CS, Liu LY. Growth behavior of lanthanum conversion coating on hot-dip galvanized steel. *Surf Coat Technol.* 2014;259:654-659.
20. Zhang KB, Zhang MM, Qiao JF. Enhancement of the corrosion resistance of zinc-aluminum chromium coating with cerium nitrate. *J Alloys Compd.* 2017;692:460-464.
21. Olivier M, Lanzutti A, Motte C. Influence of oxidizing ability of the medium on the growth of lanthanide layers on galvanized steel. *Corros Sci.* 2010;52(4):1428-1439.
22. Socha RP, Franssaer J. Mechanism of formation of silica-silicate thin films on zinc. *Thin Solid Films.* 2005;488(1-2):45-55.
23. Zhang SH, Kong G, Sun Z, Che CS, Lu JT. Effect of formulation of silica-based solution on corrosion resistance of silicate coating on hot-dip galvanized steel. *Surf Interface Anal.* 2016;48(3):132-138.
24. Zhang X, van den Bos C, Sloof WG, Hovestad A, Terryn H, de Wit JHW. Comparison of the morphology and corrosion performance of Cr (VI)- and Cr (III)-based conversion coatings on zinc. *Surf Coat Technol.* 2005;199(1):92-104.
25. Saarima V, Kauppinen E, Markkula A, Juhanoja J, Skrifvars B-J, Steen P. Microscale distribution of Ti-based conversion layer on hot dip galvanized steel. *Surf Coat Technol.* 2012;206(19-20):4173-4179.
26. Szczygieł B, Winiarski J, Tylus W. Effect of deposition time on morphology, corrosion resistance and mechanical properties of Ti-containing conversion coatings on zinc. *Mater Chem Phys.* 2011;129(3):1126-1131.
27. Sinapi F, Forget L, Delhalle J, Mekhalif Z. Formation and characterization of thin films of  $H(CH_2)_xPO(OH)_2$  on polycrystalline zinc substrates. *Surf Interface Anal.* 2002;34(1):148-154.
28. Ogle K, Tomandl A, Meddahi N, Wolpers M. The alkaline stability of phosphate coatings I: ICP atomic emission spectroelectrochemistry. *Corros Sci.* 2004;46(4):979-995.
29. Tomandl A, Wolpers M, Ogle K. The alkaline stability of phosphate coatings II: in situ Raman spectroscopy. *Corros Sci.* 2004;46(4):997-1011.
30. Forsyth M, Hinton B (Eds). *Rare earth-based corrosion inhibitors*. Amsterdam: Elsevier; 2014.
31. Popov BN. *Corrosion Engineering, Principles and Solved Problems*. Amsterdam: Elsevier; 2015.
32. Dobryszycy J, Bialozor S. On some organic inhibitors of zinc corrosion in alkaline media. *Corros Sci.* 2001;43(7):1309-1319.
33. Stupnišek-Lisac E, Podbršček S. Non-toxic organic zinc corrosion inhibitors in hydrochloric acid. *J Appl Electrochem.* 1994;24(8):779-784.
34. Morad MS. Inhibition of phosphoric acid corrosion of zinc by organic onium compounds and their adsorption characteristics. *J Appl Electrochem.* 1999;29(5):619-626.
35. Kartsonakis IA, Stanciu SG, Matei AA, Hristu R, Karantonis A, Charitidis CA. A comparative study of corrosion inhibitors on hot-dip galvanized steel. *Corros Sci.* 2016;112:289-307.
36. Rudresh HB, Mayanna SM. The synergistic effect of halide ions on the corrosion inhibition of zinc by n-decylamine. *Corros Sci.* 1979;19(6):361-370.
37. Talati JD, Desai MN, Shah NK. Meta-substituted aniline-N-salicylidenes as corrosion inhibitors of zinc in sulphuric acid. *Mater Chem Phys.* 2005;93(1):54-64.
38. Georges C, Rocca E, Steinmetz P. Synergistic effect of toluotriazol and sodium carboxylates on zinc corrosion in atmospheric condition. *Electrochim Acta.* 2008;53(14):4839-4845.
39. El-Sayed AR, Harm U, Mangold KM, Fürbeth W. Protection of galvanized steel from corrosion in NaCl solution by coverage with phytic acid SAM modified with some cations and thiols. *Corros Sci.* 2012;55:339-350.
40. Azaroual MA, El Harrak EF, Touir R, Rochdi A, Ebn Touhami M. Synergistic corrosion protection for galvanized steel in 3.0% NaCl solution by sodium gluconate and cationic surfactant. *J Mol Liq.* 2016;220:549-557.
41. Bawazeera TM, El Defrawy AM, El-Shafei AA. Corrosion inhibition of zinc in sodium sulphate solution using nonionic surfactants of tween series: experimental and theoretical study. *Colloids Surf A: Physicochem Eng Aspects.* 2017;520:694-700.
42. Qiang Y, Zhang S, Guo L, et al. Sodium dodecyl benzene sulfonate as a sustainable inhibitor for zinc corrosion in 26%  $NH_4Cl$  solution. *J Clean Prod.* 2017;152:17-25.
43. Lebrini M, Fontaine G, Gengembre L, Traisnel M, Lerasle O, Genet N. Corrosion protection of galvanized steel and electroplating steel by decanoic acid in aqueous solution: electrochemical impedance spectroscopy, XPS and ATR-FTIR. *Corros Sci.* 2009;51(6):1201-1206.
44. Peultier J, Rocca E, Steinmetz J. Zinc carboxylating: a new conversion treatment of zinc. *Corros Sci.* 2003;45(8):1703-1716.
45. Aramaki K. Prevention of zinc corrosion in oxygenated 0.5 M NaCl by treatment in a cerium (III) nitrate solution and modification with sodium hexadecanoate. *Corros Sci.* 2006;48(10):3298-3308.
46. Rammelt U, Koehler S, Reinhard G. Electrochemical characterisation of the ability of dicarboxylic acid salts to the corrosion inhibition of mild steel in aqueous solutions. *Corros Sci.* 2011;53(11):3515-3520.
47. Rammelt U, Köhler S, Excor R. EIS characterization of the inhibition of mild steel corrosion with carboxylates in neutral aqueous solution. *Electrochim Acta.* 2008;53(23):6968-6972.
48. Aramaki K. Effects of organic inhibitors on corrosion of zinc in an aerated 0.5 M NaCl solution. *Corros Sci.* 2001;43(10):1985-2000.
49. Reinhard G, Radtke M, Rammelt U. On the role of the salts of weak acids in the chemical passivation of iron and steel in aqueous solutions. *Corros Sci.* 1992;33(2):307-313.
50. Lebrini M, Traisnel M, Gengembre L, Fontaine G, Lerasle O, Genet N. Electrochemical impedance spectroscopy and X-ray photoelectron spectroscopy study of the corrosion behaviour of galvanized steel and electroplating steel. *Appl Surf Sci.* 2011;257(8):3383-3387.

51. Taheri P, Wielant J, Hauffman T, et al. A comparison of the interfacial bonding properties of carboxylic acid functional groups on zinc and iron substrates. *Electrochim Acta*. 2011;56(4):1904-1911.
52. Taheri P, Lill K, de Wit JHW, et al. Effects of zinc surface acid-based properties on formation mechanisms and interfacial bonding properties of zirconium-based conversion layers. *J Phys Chem C*. 2012;116(15):8426-8436.
53. Smith MB. *Organic Chemistry: An Acid-Base Approach*. 2nd ed. Boca Raton: CRC Press, Taylor & Francis Group; 2016.
54. Ovarfort R. New electrochemical cell for pitting corrosion testing. *Corros Sci*. 1988;28(2):135-140.
55. Pourbaix M. *Atlas of Electrochemical Equilibria in Aqueous Solutions*. 2nd ed. Huston: National Association of Corrosion; 1974.
56. Muster TH, Cole IS. The protective nature of passivation films on zinc: surface charge. *Corros Sci*. 2004;46(2):2319-2335.
57. Degen A, Kosec M. Effect of pH and impurities on the surface charge of zinc oxide in aqueous solution. *J Europ Cer Soc*. 2000;20(6):667-673.
58. Cachet C, Ganne F, Maurin G, Petitjean J, Vivier V, Wiart R. EIS investigation of zinc dissolution in aerated sulfate medium. Part I: bulk zinc. *Electrochim Acta*. 2001;47(3):509-518.
59. Cachet C, Ganne F, Joiret S, et al. EIS investigation of zinc dissolution in aerated sulphate medium. Part II: zinc coatings. *Electrochim Acta*. 2002;47(21):3409-3422.
60. Ferreira JM Jr, Oliveira M, Trindade GF, Santos LCL, Tomachuk CR, Baker MA. Development and characterisation of zinc oxalate conversion coatings on zinc. *Corros Sci*. 2018;137:13-32.
61. Liu YW, Wang ZY, Cao GW, Cao Y, Huo Y. Study on corrosion behavior of zinc exposed in coastal-industrial atmospheric environment. *Mater Chem Phys*. 2017;198:243-249.
62. Orazem ME, Pébère N, Tribollet B. Enhanced graphical representation of electrochemical impedance data. *J Electrochem Soc*. 2006;153(4):B129-B136.
63. Barcia OE, D'Elia E, Frateur I, Mattos OR, Pébère N, Tribollet B. Application of the impedance model of de Levie for the characterization of porous electrodes. *Electrochim Acta*. 2002;47(13-14):2109-2116.
64. Alexander CL, Tribollet B, Vivier V, Orazem ME. Contribution of surface distributions to constant-phase-element (CPE) behavior: 3. Adsorbed Intermediates. *Electrochim Acta*. 2017;251:99-108.
65. Hirschorn B, Orazem ME, Tribollet B, Vivier V, Frateur I, Musiani M. Constant-phase-element behavior caused by resistivity distributions in films. II Applications. *J Electrochem Soc*. 2010;157(12):C458-C463.
66. Hirschorn B, Orazem ME, Tribollet B, Vivier V, Frateur I, Musiani M. Determination of effective capacitance and film thickness from constant-phase-element parameters. *Electrochim Acta*. 2010;55(21):6218-6227.
67. Alexander CL, Tribollet B, Orazem ME. Influence of micrometric-scale electrode heterogeneity on electrochemical impedance spectroscopy. *Electrochim Acta*. 2016;201:374-379.
68. Volovitch P, Allely C, Ogle K. Understanding corrosion via corrosion product characterization: I. Case study of the role of Mg alloying in Zn-Mg coating on steel. *Corros Sci*. 2009;51(6):1251-1262.
69. Srivastava OK, Secco EA. Studies on metal hydroxy compounds. II. Infrared spectra of zinc derivatives  $\epsilon$ -Zn(OH)<sub>2</sub>,  $\beta$ -ZnOHCl, ZnOHF-, Zn<sub>5</sub>(OH)<sub>8</sub>Cl<sub>2</sub>, and Zn<sub>5</sub>(OH)<sub>8</sub>Cl<sub>2</sub>·H<sub>2</sub>O. *Can J Chem*. 1967;46(6):585-588.
70. Persson D, Thierry D, LeBozec N, Prosek T. In situ infrared reflection spectroscopy studies of the initial atmospheric corrosion of Zn-Al-Mg coated steel. *Corros Sci*. 2013;72:54-63.
71. LeBozec N, Thierry D, Rohwerder M, Persson D, Luckeneder G, Luxem L. Effect of carbon dioxide on the atmospheric corrosion of Zn-Mg-Al coated steel. *Corros Sci*. 2013;74:379-386.
72. Woll C. The chemistry and physics of zinc oxide surfaces. *Prog Surf Sci*. 2007;82(2-3):55-120.
73. Diler E, Rioual S, Lescop B, Thiery D, Rouvellou B. Chemistry of corrosion products of Zn and MgZn pure phases under atmospheric conditions. *Corros Sci*. 2012;65:178-186.
74. Chen YY, Chung SC, Shih HC. Studies on the initial stages of zinc atmospheric corrosion in the presence of chloride. *Corros Sci*. 2006;48(11):3547-3564.
75. Czakis-Sulikowska D, Czylikowska A. Complexes of Mn(II), Co(II), Ni(II) and Cu(II) with 4,4'-bipyridine and dichloroacetates synthesis, thermal and other properties. *J Thermal Anal Cal*. 2003;71(1):395-405.
76. Vargová Z, Almási M, Arabuli L, Györyová K, Zeleňák V, Kuchár J. Utilization of IR spectral detailed analysis for coordination mode determination in novel Zn-cyclen-aminoacid complexes. *Spectrochim Acta Part aA*. 2011;78(2):788-793.
77. Shamsipur M, Pourmortazavi SM, Hajimirsadeghi SS, Zahedi MM, Rahimi-Nasrabadi M. Facile synthesis of zinc carbonate and zinc oxide nanoparticles via direct carbonation and thermal decomposition. *Ceram Int*. 2013;39(1):819-827.
78. Pourmortazavi SM, Marashianpour Z, Karimi MS, Mohammad-Zadeh M. Electrochemical synthesis and characterization of zinc carbonate and zinc oxide nanoparticles. *J Mol Struct*. 2015;1099:232-238.
79. Liang J, Hu Y, Wu Y, Chen H. Fabrication and corrosion resistance of superhydrophobic hydroxide zinc carbonate film on aluminum substrates. *J Nanomaterials*. 2013;2013:1-6. Article Id 139768
80. Zeleňák V, Várgov Z, Györyová K. Correlation of infrared spectra of zinc(II) carboxylates with their structures. *Spectrochim Acta Part aA*. 2007;66(2):262-272.
81. Simon-Kutscher J, Gericke A, Hühnerfuss H. Effect of bivalent Ba, Cu, Ni, and Zn cations on the structure of octadecanoic acid monolayers at the air-water interface as determined by external infrared reflection-absorption spectroscopy. *Langmuir*. 1996;12(4):1027-1034.
82. Lewandowski W, Kalinowska M, Lewandowska H. The influence of metals on the electronic system of biologically important ligands. Spectroscopic study of benzoates, salicylates, nicotines and isoorotates. *J Inorg Biochem*. 2005;99(7):1407-1423.
83. Suedile F, Robert F, Roos C, Lebrini M. Corrosion inhibition of zinc by Mansoa alliacea plant extract in sodium chloride media: extraction, characterization and electrochemical studies. *Electrochim Acta*. 2014;133:631-638.

**How to cite this article:** Fedel M, Poelman M, Olivier M, Deflorian F. Sebacic acid as corrosion inhibitor for hot-dip galvanized (HDG) steel in 0.1 M NaCl. *Surf Interface Anal*. 2019;51:541-551. <https://doi.org/10.1002/sia.6617>